

Assessment of low-velocity impact damage in composites by the measure of second-harmonic guided waves with the phase-reversal approach

Science Progress

2020, Vol. 103(1) 1–14

© The Author(s) 2020

Article reuse guidelines:

sagepub.com/journals-permissions

DOI: 10.1177/0036850419881079

journals.sagepub.com/home/sci

Weibin Li¹ , Chang Jiang¹, Xinlin Qing¹,
Liangbing Liu² and Mingxi Deng² 

¹School of Aerospace Engineering, Xiamen University, Xiamen, China

²College of Aerospace Engineering, Chongqing University, Chongqing, China

Abstract

Structural strength and integrity of composites can be considerably affected by the low-velocity impact damage due to the unique characteristics of composites, such as layering bonded by adhesive and the weakness to impact. For such damage, there is an urgent need to develop advanced nondestructive testing approaches. Despite the fact that the second harmonics could provide information sensitive to the structural health condition, the diminutive amplitude of the measured second-order harmonic guided wave still limits the applications of the second-harmonic generation-based nonlinear guided wave approach. Herein, laminated composites suffered from low-velocity impact are characterized by use of nonlinear guided waves. An enhancement in the signal-to-noise ratio for the measure of second harmonics is achieved by a phase-reversal method. Results obtained indicate a monotonic correlation between the impact-induced damage in composites and the relative acoustic nonlinear indicator of guided waves. The experimental finding in this study shows that the measure of second-order harmonic guided waves with a phase-reversal method can be a promising indicator to impact damage rendering in an improved and reliable manner.

Keywords

Composites, low-velocity impact, second-harmonic generation, phase reversal, ultrasonic guided waves

Corresponding author:

Mingxi Deng, College of Aerospace Engineering, Chongqing University, Chongqing 400044, China.

Email: dengmx65@yahoo.com



Creative Commons Non Commercial CC BY-NC: This article is distributed under the terms of the Creative Commons Attribution-NonCommercial 4.0 License (<https://creativecommons.org/licenses/by-nc/4.0/>)

which permits non-commercial use, reproduction and distribution of the work without further permission provided the original work is attributed as specified on the SAGE and Open Access pages (<https://us.sagepub.com/en-us/nam/open-access-at-sage>).

Introduction

Prevalence of composites is found in the industrial field of aircraft, transportation, and marine owing to their superior material properties.¹ However, since the composite laminates often lack the through-thickness reinforcement that can subject to impact in the transverse direction, such structure has low transverse damage tolerance.² For low-velocity impacts in the composite, laminated structures absorb the impact energy without plastic deformation.^{3–5} Defects existing in the inner layers of composite laminates caused by impact are complex and cannot easily be detected effectively. Recently, transverse stresses and plasticity propagation in layered structures were analyzed by Liu and Jeffers.^{6,7} Invisible interior defects caused by low-velocity impacts will degrade the structural performance of composite laminates.^{8,9} With the impact-induced damage affecting significantly the composite materials, failures to evaluate and characterize the low-velocity impacts will result in unpredictable catastrophes of the composite structure. Therefore, nondestructive testing (NDT) approaches need to be developed for the damage assessment of low-velocity impacts.

Numerous NDT techniques were used for the assessment of impact damage in composite laminates.¹⁰ Impact-induced delamination in such materials was imaged by digital shearography,¹¹ which demands sensitive and expensive instruments as well as highly skilled inspectors for the use of this technique. In addition, the lack of clarity of defects deep beneath the surface also limits the application. Recently, a combination of the tomographic and optical techniques was used to evaluate the impact damage in composites by Sfarra and colleagues.^{12,13} Radiographic testing is another approach for damage inspection in composites.¹⁴ However, the radiographic approach is only available in the case of delamination with specific orientation as regards X-ray beam. Ultrasonic testing is an effective method for impact damage detection in composites. However, most earlier investigations are about macro-damage detection by use of linear ultrasonic waves.¹⁵ The nonlinear acoustic approach has been taken as a promising means for the assessment of micro-damage.^{16–18} Another investigation on impact damage detection was conducted in a sandwich plate by Meo and Zumpano.¹⁹ Aymerich and Staszewski²⁰ investigated the relevance of impact energy and sidebands of ultrasonic amplitude by frequency modulation of ultrasonic waves in composite laminates. Progressive damage in polymer-based composites was monitored by nonlinear dynamics and the acoustic emission technique.²¹

Recently, considering the great advantages of the guided wave technique for material characterization, many applications have been realized to detect and evaluate delamination, stress fatigue, thermal fatigue, and impact damage in composite materials by guided waves.^{22–26} Favorable characteristics of guided wave techniques comprise remarkable cost-effectiveness and low energy consumption.^{22,27} Recently, increasing attention has been paid to NDT in composites by nonlinear guided waves. Generation of higher harmonic waves is the typical ultrasonic nonlinear phenomenon. Second-harmonic generation (SHG) of guided waves in metallic materials was reported in earlier publications.^{28–31} An experimental scheme for

characterizing the thermal damage was developed by SHG of Lamb waves in composites.³² Second-harmonic guided waves were also adopted to investigate the potential of fatigue assessment in composites.³³ To the authors' knowledge, SHG of guided waves is a sensitive indicator for composite structural health condition at an early stage.

Nevertheless, SHG of guided waves in composites can be readily omitted for the reason of a very small amplitude of measured second-harmonic signals. Accordingly, it is practically difficult to implement the nonlinear guided wave technique for the reason of low generation efficiency of second harmonics. In view of this difficulty, a phase-reversal approach is employed to intensify the signal clarity of SHG. Second-harmonic signals of a phase-matched guided wave are measured in this study. In addition, we extracted the second harmonics after the superposition of two propagating guided waves with the opposite phase. The method proposed is used for the damage assessment in the tested specimens. Variations of the acoustic nonlinear parameter corresponding to different artificial impact energies are obtained in the composite structures. Variations of wave velocity and acoustic nonlinearity with respect to impact energies are provided as well.

General considerations

The nonlinear feature of guided waves

The nonlinearity of materials is related to various imperfections in the material microstructure or discontinuities of interfaces.^{34,35} Distortion of ultrasonic waveforms occurs in tested materials with damage, and double-frequency second-harmonic waves are subsequently generated. The damage-induced acoustic nonlinearity (expressed as β) can be qualitatively expressed as^{31,32,35}

$$\beta = \frac{8}{k^2 x} \cdot \frac{A_2}{A_1^2} F_u \quad (1)$$

where β is the acoustic nonlinear parameter; k denotes the wavenumber; the amplitudes of the primary wave and the second-harmonic one are represented by A_1 and A_2 at the given propagation distance x , respectively; and F_u is the feature function,³⁵ which can be considered as a constant in this work. Thus, the measurable value of A_2/A_1^2 denotes the relative acoustic nonlinear parameter (expressed as $\tilde{\beta}$) to evaluate the damage-induced material nonlinearity, that is

$$\tilde{\beta} = \frac{A_2}{A_1^2} \propto \beta x \quad (2)$$

As shown above, $\tilde{\beta}$ is in direct proportion to the acoustic nonlinear parameter β . It is also found that the relative nonlinear parameter $\tilde{\beta}$ linearly increases with x . This cumulative effect is essential and unique for nonlinear guided wave testing, to ensure that the measured acoustic nonlinearity relating to material nonlinearity arises in the experimental measurement.²⁸⁻³²

Principle of the phase-reversal approach

The phase-reversal method is an effective means to counteract odd harmonics while highlighting the contribution of the even ones.^{36,37} The fundamental of the phase-reversal method presented in this study expands to only the second-order nonlinear term. The total wavefield regarding guided wave propagation in specimens with nonlinearity is

$$u^{(0)} = A_1 \exp[j(kx - \omega t)] + A_2 \exp[2j(kx - \omega t)] \quad (3)$$

where $u^{(0)}$ is the displacement field of guided waves with an initial phase propagation in the specimens. The displacement field of elastic waves in solid media can be expressed as the exponential function with the virtual power exponent j , t is the variable of time, and ω is the angular frequency.

With the phase of the fundamental ultrasonic wave reversed 180°, while retaining the remaining conditions, the total wavefield in the waveguide is

$$u^{(\pi)} = A_1 \exp[j(kx - \omega t + \pi)] + A_2 \exp[2j(kx - \omega t + \pi)] \quad (4)$$

By summing equations (3) and (4), one can see that only the second-harmonic field is left as shown below

$$\tilde{u} = u^{(0)} + u^{(\pi)} = 2A_2 \exp[2j(kx - \omega t)] \quad (5)$$

It is shown that the phase-reversal technique doubles the second-harmonic amplitude while counteracting that of the primary ones. Apparently, the efficiency of SHG of primary guided wave propagation can be effectively enhanced by employing the phase-reversal method proposed here in nonlinear media.

Mode selection and signal excitation

Guided wave propagation in the composite structure has a few unique features due to anisotropic properties, such as direction-dependent wave speeds. In addition, many factors (e.g. thickness, density, and elastic properties) can affect the guided waves propagating in composites. Phase and group velocity dispersion curves play a critical role in mode selection and frequency tuning of guided wave NDT. In composite laminates, guided wave propagation can be described by satisfying Navier's displacement equations within each layer. A transfer matrix, which relates the displacement and stress of each layer, can be constructed to represent the relations. In this study, the classical transfer matrix method is employed to calculate the dispersion curves of guided waves in the tested composite samples (shown in Figure 1).

As one can see from Figure 1, the selected phase-matched modes comprise the fundamental $S1$ mode waves (2.5 MHz) and the double-frequency $S2$ mode (5.0 MHz). The phase velocity (9.70 km/s) of the primary mode is equal to that of the second-order one, so does the group velocity (9.50 km/s).

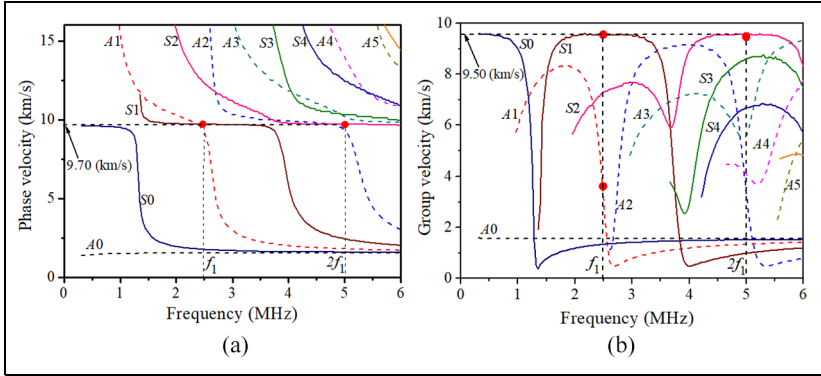


Figure 1. Dispersion curves of (a) phase velocity and (b) group velocity. Wave propagation is along the fiber direction of the unidirectional composites.

In general, the dispersive nature of guided waves negatively affects the SHG. Thus, cumulative SHG versus propagation distance is crucial to measure the nonlinear response of guided waves.³⁰ The second harmonics of guided waves synchronize with the primary waves, which results in the cumulative phenomenon of SHG. More detailed discussions on this issue can be found in our earlier work.³² In this investigation, *S1* mode meets the condition of internal resonance (i.e. its phase and group velocity equal those of the double-frequency second-harmonic wave, as indicated in Figure 1), which ensures the cumulative effect of SHG.

In this study, excitation and reception of guided wave signals are realized by piezoelectric (PZT) transducers. The wave incident angle (θ) in wedges can be calculated as

$$\theta = \sin^{-1}\left(\frac{c_l}{c_p}\right) \quad (6)$$

where c_p denotes the phase velocity of the expected *S1* mode and c_l is the wave velocity in the wedge material.

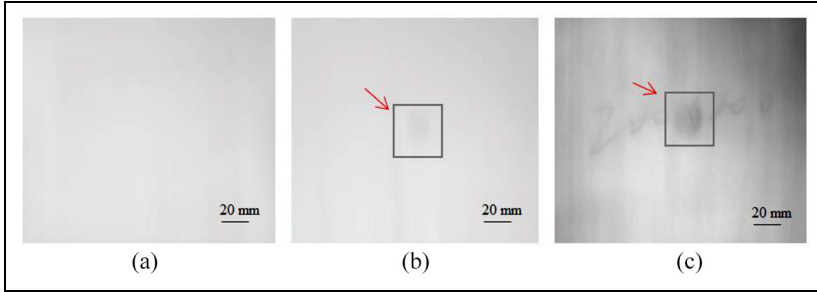
Experiments

Specimens

The experimental tests were carried out in carbon fiber lay-up architectures, of which the size is 1.0 mm thick, 200 mm long, and 200 mm wide. The specimens used in this study are provided by the same supplier (Beijing Institute of Aeronautical Materials). Mass density and elastic constants of the tested specimen are provided in Table 1. The stiffness matrix is obtained by referencing the GB/T 1477 standard. One of the specimens is undamaged for the reference experiment. The low-velocity impact damage was induced by an MTS free-fall drop test machine (CEAST 9340;

Table 1. Mass density ρ (in g/cm^3) and elastic constants (in GPa) of the tested composites.

ρ	C_{11}	C_{12}	C_{13}	C_{22}	C_{23}	C_{33}	C_{44}	C_{55}	C_{66}
1.58	148	4.11	4.11	10.60	3.10	10.60	3.75	7.20	7.20

**Figure 2.** Infrared thermography of the impact damage in (a) virgin specimen, (b) 5 J impact loading specimen, and (c) 15 J impact loading specimen.

Instron), conforming to the ASTM D7136 standard. The impactor weighs 2.50 kg with a smooth hemispherical striker, of which the diameter is 16 mm. In this research, composite laminates were placed in the middle of the tested machine. The impact energies are calculated according to the falling height of the striker from the top of the crosshead at resting position on each sample. The impact energies of 5.0 and 15 J were derived from the gravitational potential energy equations referencing the ASTM D7136 standard.

The impact-induced damage in the specimens was also inspected by the infrared thermography technique, as illustrated in Figure 2. It is shown that the impact damage can hardly be found in the specimens even by infrared thermography.

The system setup

An experimental setup is provided in Figure 3. A sinusoidal tone-burst electrical signal (2.50 MHz) is excited by a RITEC system, which then passes through a 14-dB attenuator and a low pass filter. A narrow band transmitter T_x (central frequency at 2.25 MHz) is employed for the generation of the primary wave. The other broad-band PZT transducer (central frequency at 5.0 MHz) is taken as a receiver R_x to measure the primary waves and the generated second harmonics concurrently. The transducers were clamped to the acrylic wedges. A light lubrication oil (type: Ultragel II; Sonotech) was used to facilitate the transmission of sound energy between different media. The transducers were mounted on the specimens with the couplant. The relative acoustic nonlinear parameters (A_2/A_1^2) of the guided waves

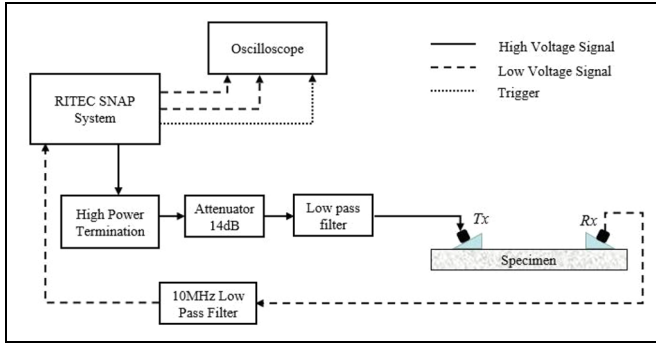


Figure 3. Experimental setup.

in the intact sample were examined first at different propagation distances varying every 10 mm from 40 to 80 mm between the two transducers. Time-domain signals were displayed first in the digital oscilloscope, and then the frequency-domain signals were obtained by fast Fourier transform (FFT). Eventually, the two impact-damaged samples were tested under the same conditions by the above ultrasonic test system.

Results and discussion

As analyzed in section “Mode selection and signal excitation,” the phase-matched mode pair selected is crucial for nonlinear ultrasonic guided wave testing. Thus, the group velocity of the propagating signal was measured and compared with the theoretical value. Besides, the frequency of the measured signal was checked to ensure that it is the expected guided wave mode. Practically, the $A1$ mode is very likely to be generated when the $S1$ mode is to be excited owing to their adjacent positions as shown in Figure 1(a). But it is also noticed that their group velocities differ from each other, so the wave package of the double-frequency harmonic signal ($S1$ mode) will eventually separate from the $A1$ mode wave package due to the noticeable group velocity difference.³² The typical measured signals were modulated by Hanning window and occupy a length of 16 cycles, as illustrated in Figure 4(a). Figure 4(b) shows the frequency spectrum obtained by the FFT of measured signals. As one can see, group velocity (expressed as c_g) of the received propagating signal is 9.43 km/s, and its central frequency is 2.50 MHz. Thus, the expected guided wave mode can be confirmed.

Figure 5(a) clearly presents the frequency spectra of primary guided waves and second harmonics. In addition, as indicated in equation (2), the relative nonlinear parameter (the ratio of measured amplitudes) versus wave propagation distance can be constructed to demonstrate nonlinearity. The cumulative effect mentioned previously was confirmed by Figure 5(b). In the experiment, the amplitude ratio of second harmonics to the second power of the primary one, which could generally

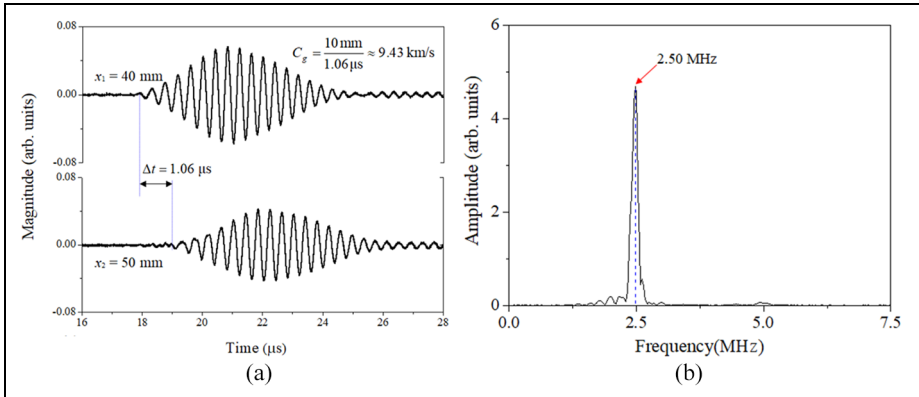


Figure 4. Confirmation of (a) group velocity and (b) frequency spectrum of the measured signal.

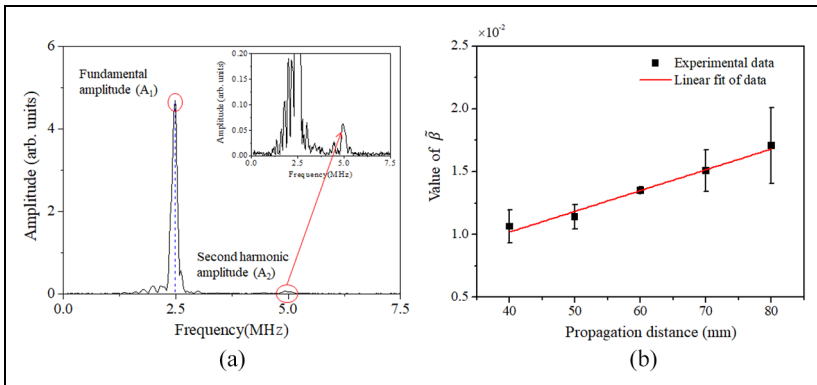


Figure 5. (a) Frequency spectra of the measured signal at a specific position and (b) relative nonlinear parameters measured at different propagation distances.

be expressed as the relative acoustic nonlinearity as indicated in equation (2), is measured three times at each marked distance. The experimental average values with error bars are presented in Figure 5(b), which suggested a monotonic relationship with the propagation distance. Generally, SHG of guided wave propagation can be affected by coupling media, instruments, and material damage. It is noted that the effects of coupling media and instruments can be minimized by representing acoustic nonlinearity as the slope ratio of the measured $\tilde{\beta}$ versus propagation distance.^{32,35}

The effect of the phase-reversal approach was also examined. Here we show a specific implementation process. For the undamaged specimen, a sine pulse wave at

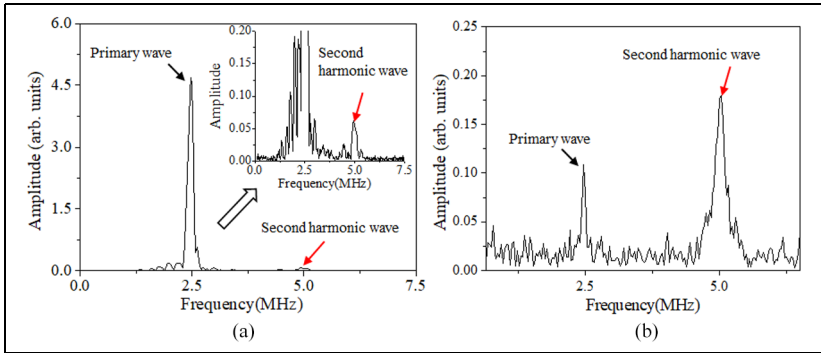


Figure 6. Frequency spectra of the measured guided wave signal by (a) the normal operation and (b) the phase-reversal method.

the frequency of 2.50 MHz was applied to the incident transducer. All the settings are kept unchanged except for a phase-reversal step of the primary waves excited from the incident transducer and then the same measurement is repeated. Obviously, after superposition of these two phase-reversed signals, the signals with opposite phases can be counteracted, while signals in phase with each other will be enhanced as illustrated in section “Principle of the phase-reversal approach.” Figure 6 shows the spectra of measured signals in the frequency domain before and after the phase-reversal signal processing. The very small amplitude of the measured second harmonics is scarcely noticed in contrast to that of the primary wave under normal circumstances. However, the second-harmonic amplitude increases significantly with the phase-reversal technique adopted, while the two fundamental waves counteract each other. In detail, the second-harmonic signal (i.e. the double-frequency component) becomes twice as much as it is before. The remained primary wave amplitude does not exactly equal zero (see Figure 6(b)), which can be attributed to the inconsistent coupling conditions during the period of repeated measurements. Despite that, this technique is still able to effectively build up the second harmonics, which is favorable for the measurement of acoustic nonlinearity.

In the conventional approach, we calculate A_2/A_1^2 based on the values of primary wave amplitude and the second-harmonic one shown in Figure 6(a). As seen, the amplitude of the second harmonics is diminutive in contrast to that of the primary one, which suggests that the SHG induced by material nonlinearity is rather very small. In addition, the extraction of the second harmonics can be influenced by the fundamental waves of great magnitude. Thus, a phase-reversal technique is applied to enhance the second-harmonic signals while counteracting the primary waves to a great extent.

As indicated in equation (5), the two fundamental waves offset each other while the amplitude of the double-frequency harmonic wave has doubled by the phase-reversal method. In this method, the two time-domain signals with the opposite phase are obtained simultaneously using excitations of two out-of-phase primary

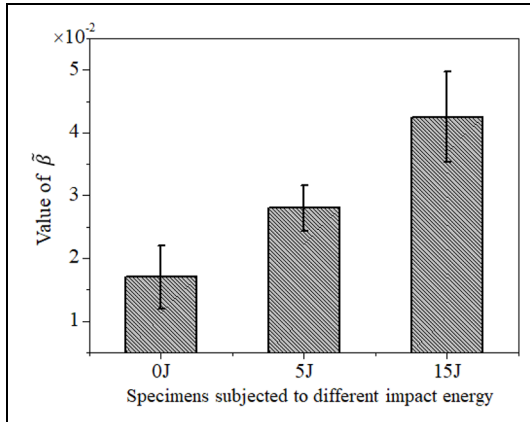


Figure 7. Relative nonlinear parameters measured in composites as a function of impact energies.

waves for a given propagation distance. Then, the primary wave amplitudes of the two signals in the frequency domain can be obtained, which are denoted by A_{1a} and A_{1b} , respectively. As regards the determination of $\tilde{\beta} = A_2/A_1^2$, A_1 is calculated through $A_1 = (A_{1a} + A_{1b})/2$. Concurrently, A_2 is obtained from the spectrum of superposition signals as shown in Figure 6(b). Based on the above measurements, the corresponding $\tilde{\beta}$ values are calculated for specimens with damage of different levels.

The experimental results indicate that the phase-reversal technique is a feasible method for the enhancement in the second-harmonic signal and thus increases the resolution for NDT evaluation of micro-damages in materials (due to higher signal-to-noise ratio (SNR) of the second-harmonic signals measured). SHG of guided waves is applied in detecting the low-velocity impact damage in composite laminates with the phase-reversal technique. Figure 7 provides us with the correlation of impact energies and the relative nonlinear parameter measured by the above experiment. As the impact energies increase, the relative acoustic nonlinear parameter increases significantly.

With regard to the sensitivity analysis of c_g and $\tilde{\beta}$ to impact damage, Figure 8 presents the variations of group velocities and acoustic nonlinearity with respect to different impact energies in the tested specimen. For clarity (i.e. to present only relative changes) of the results, normalizations have been implemented for all the measured acoustic parameters by referring to that of the raw materials. Since the wave velocity in the specimens under different impact energies barely varies, it is believed that c_g is insufficiently sensitive to characterize the low-velocity impact damage.

For low-velocity impacts in the composite, laminated structures absorb the impact energy without plastic deformation. Defects existing in the inner layers of

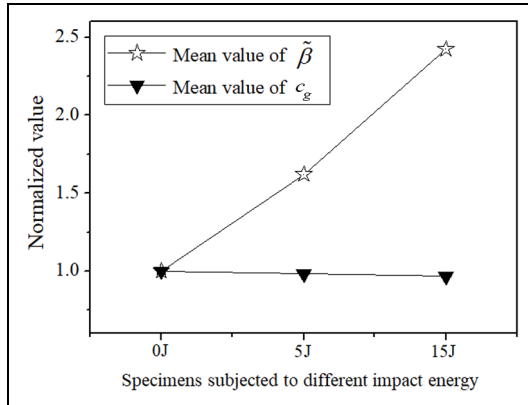


Figure 8. Variations of c_g and $\tilde{\beta}$ with respect to impact energies in tested specimens.

composite laminates caused by impact are complex and cannot easily be detected effectively. Thus, matrix cracks, delamination, fiber breakage, as well as penetration can be initiated inside the composite structures.³⁸ The low-velocity impact-induced internal damage can be the source of material nonlinearity. Distortion of the ultrasonic waveform occurs in the tested material with damage, and double-frequency second-harmonic waves are subsequently generated. Thus, the measure of SHG is a convincing means to qualitatively assess the damage induced by low-velocity impact.

Conclusion

Low-velocity impact damage in composites is detected by the SHG of ultrasonic guided waves. The second harmonics with cumulative effect versus propagation distance are generated by the phase-matched guided wave mode pair. The applicability of the chosen mode is verified experimentally. An enhancement in the SNR for the measure of second harmonics is achieved by a phase-reversal method. The proposed method is applied to assess the different levels of low-velocity impact energies in the composites. An increase in the acoustic nonlinear parameter with respect to the impact energies is observed experimentally, while velocity variations can be neglected. This work suggests that the measure of SHG combined with the phase-reversal method is a potential technique for the assessment of low-velocity impact damage in composites.


Declaration of conflicting interests


The author(s) declared no potential conflicts of interest with respect to the research, authorship, and/or publication of this article.

Funding

The author(s) disclosed receipt of the following financial support for the research, authorship, and/or publication of this article: This work was supported by the National Natural Science Foundation of China (Grant Nos 11774295, 11834008, and 11474361).

ORCID iDs

Weibin Li  <https://orcid.org/0000-0002-8925-6365>

Mingxi Deng  <https://orcid.org/0000-0001-9522-4039>

References

1. Li W, Xu C and Cho Y. Characterization of degradation progressive in composite laminates subjected to thermal fatigue and moisture diffusion by Lamb waves. *Sensors* 2016; 16: 260.
2. Mlyniec A, Korta J, Kudelski R, et al. The influence of the laminate thickness, stacking sequence and thermal aging on the static and dynamic behavior of carbon/epoxy composites. *Compos Struct* 2014; 118: 208–216.
3. Richardson MOW and Wisheart MJ. Review of low-velocity impact properties of composite materials. *Compos Part A-Appl S* 1996; 27: 1123–1131.
4. Wang S, Wu L and Ma L. Low-velocity impact and residual tensile strength analysis to carbon fiber composite laminates. *Mater Des* 2010; 31: 118–125.
5. Boccardi S, Meola C, Carlomagno GM, et al. Effects of interface strength gradation on impact damage mechanisms in polypropylene/woven glass fabric composites. *Compos Part B-Eng* 2016; 90: 179–187.
6. Liu N and Jeffers AE. Isogeometric analysis of laminated composite and functionally graded sandwich plates based on a layerwise displacement theory. *Compos Struct* 2017; 176: 143–153.
7. Liu N and Jeffers AE. Adaptive isogeometric analysis in structural frames using a layer-based discretization to model spread of plasticity. *Compos Struct* 2018; 196: 1–11.
8. Shi Y, Pinna C and Soutis C. Modelling impact damage in composite laminates: a simulation of intra- and inter-laminar cracking. *Compos Struct* 2014; 114: 10–19.
9. Choi H, Wu HT and Chang F. A new approach toward understanding damage mechanisms and mechanics of laminated composites due to low-velocity impact: part 2-analysis. *J Compos Mater* 1991; 25: 1012–1038.
10. Meyendorf NGH, Nagy PB and Rokhlin S. *Nondestructive material characterization: with applications to aerospace materials*. Berlin: Springer, 2013.
11. Kim G, Hong S, Jhang K, et al. NDE of low-velocity impact damages in composite laminates using ESPI, digital shearography and ultrasound C-scan techniques. *Int J Precis Eng Man* 2012; 13: 869–876.
12. Zhang H, Sfarra S, Sarasini F, et al. Impact modeling and a posteriori non-destructive evaluation of homogeneous particleboards of sugarcane bagasse. *J Nondestruct Eval* 2018; 37: 6.
13. Sfarra S, Lopez F, Sarasini F, et al. Analysis of damage in hybrid composites subjected to ballistic impacts: an integrated nondestructive approach. In: Thakur V, Thakur M and Kessler M (eds) *Handbook of composites from renewable materials, physico-chemical and mechanical characterization*. New York: Wiley, 2017, pp. 175–210.

14. Jones TS, Polansky D and Berger H. Radiation inspection methods for composites. *NDT Int* 1988; 21: 277–282.
15. Jhang KY. Nonlinear ultrasonic techniques for nondestructive assessment of micro-damage in material: a review. *Int J Precis Eng Man* 2009; 10: 123–135.
16. Li W, Cho Y, Lee J, et al. Assessment of heat treated Inconel X-750 alloy by nonlinear ultrasonics. *Exp Mech* 2013; 53: 775–781.
17. Nagy PB. Fatigue damage assessment by nonlinear ultrasonic material characterization. *Ultrasonics* 1998; 36: 375–381.
18. Cantrell JH and Yost WT. Nonlinear ultrasonic characterization of fatigue microstructures. *Int J Fatigue* 2001; 23: 487–490.
19. Meo M and Zumpano G. Nonlinear elastic wave spectroscopy identification of impact damage on a sandwich plate. *Compos Struct* 2005; 71: 469–474.
20. Aymerich F and Staszewski WJ. Impact damage detection in composite laminates using nonlinear acoustics. *Compos Part A-Appl S* 2010; 41: 1084–1092.
21. Bentahar M and Guerjouma RE. Monitoring progressive damage in polymer-based composite using nonlinear dynamics and acoustic emission. *J Acoust Soc Am* 2008; 125: EL39–EL44.
22. Alleyne DN and Cawley P. The interaction of Lamb waves with defects. *IEEE T Ultrason Ferr* 1992; 39: 381–397.
23. Seale MD, Smith BT and Prosser WH. Lamb wave assessment of fatigue and thermal damage in composites. *J Acoust Soc Am* 1998; 103: 2416–2424.
24. Katunin A, Dragan K and Dziendzikowski M. Damage identification in aircraft composite structures: a case study using various non-destructive testing technique. *Compos Struct* 2015; 127: 1–9.
25. Wang L and Yuan F. Group velocity and characteristic wave curves of Lamb waves in composites: modeling and experiments. *Compos Sci Technol* 2007; 67: 1370–1384.
26. Rogge MD and Leckey CA. Characterization of impact damage in composite laminates using guided wavefield imaging and local wavenumber domain analysis. *Ultrasonics* 2013; 53(7): 1217–1226.
27. Chimenti DE. Guided waves in plates and their use in materials characterization. *Appl Mech Rev* 1997; 50: 247–284.
28. Pruell C, Kim JY, Qu J, et al. A nonlinear-guided wave technique for evaluating plasticity-driven material damage in metal plate. *NDT&E Int* 2008; 42: 199–203.
29. Deng M, Wang P and Lv X. Experimental verification of cumulative growth effect of second harmonics of Lamb wave propagation in an elastic plate. *Appl Phys Lett* 2005; 86: 124104.
30. Deng M. Analysis of second harmonic generation of Lamb modes using modal analysis approach. *J Appl Phys* 2003; 94: 4152–4159.
31. de Lima WJN and Hamilton MF. Finite-amplitude waves in isotropic elastic plates. *J Sound Vib* 2003; 265: 819–839.
32. Li W, Cho Y and Achenbach JD. Detection of thermal fatigue in composites by second harmonic Lamb waves. *Smart Mater Struct* 2012; 21: 085019.
33. Rauter N, Lammering R and Kühnrich T. On the detection of fatigue damage in composites by use of second harmonic guided waves. *Compos Struct* 2016; 152: 247–258.
34. Li W, Cho Y and Hyun S. Characteristics of ultrasonic nonlinearity by thermal fatigue. *Int J Precis Eng Man* 2012; 13: 935–940.
35. Li W and Cho Y. Thermal fatigue damage assessment in an isotropic pipe using nonlinear ultrasonic guided waves. *Exp Mech* 2014; 54: 1309–1318.

36. Verbeek XA, Ledoux LA, Willigers JM, et al. Experimental investigation of the pulse inversion technique for imaging ultrasound contrast agents. *J Acoust Soc Am* 2000; 107(4): 2281–2290.
37. Kim JY, Jacobs LJ, Qu J, et al. Experimental characterization of fatigue damage in a nickel-base superalloy using nonlinear ultrasonic waves. *J Acoust Soc Am* 2006; 120: 1266–1273.
38. Balzani C and Wagner W. An interface element for the simulation of delamination in unidirectional fiber-reinforced composite laminates. *Eng Fract Mech* 2008; 75: 2597–2615.

Author biographies

Weibin Li was born in 1982. His research interests include ultrasonic nondestructive testing and nonlinear guided waves. Currently, he is working as an Associate Professor in the School of Aerospace Engineering, Xiamen University, China. He has authored over 40 refereed journal and proceedings articles.

Chang Jiang was born in 1994. He received the bachelor degree from Huazhong University of Science and Technology. He is currently studying in the School of Aerospace Engineering, Xiamen University, as a graduate student. His research interests include nonlinear ultrasonic technique.

Xinlin Qing was born in 1967. He is currently a Distinguished Professor in the School of Aerospace Engineering, Xiamen University. His research interests include multifunctional sensor network, structural health monitoring, aviation health management and smart materials and structures.

Liangbing Liu was born in 1981. He is currently a Research Fellow in the College of Aerospace Engineering, Chongqing University, China. His research interests include ultrasonic signal processing and nonlinear ultrasonics.

Mingxi Deng was born in 1965. He is currently working as a Distinguished Professor in the College of Aerospace Engineering, Chongqing University, China. His research interests includes nonlinear guided waves, ultrasonics wave propagation in complicated materials and ultrasonic nondestructive testing.